

## Nanomagnetite-Zeolite Composites in the Removal of Arsenate from Aqueous Systems

Carmen Pizarro,<sup>\*,a,b</sup> María A. Rubio,<sup>a,b</sup> Mauricio Escudey,<sup>a,b</sup> María F. Albornoz,<sup>a</sup>  
Daniela Muñoz,<sup>a</sup> Juliano Denardin<sup>b,c</sup> and José D. Fabris<sup>d,e</sup>

<sup>a</sup>Facultad de Química y Biología, <sup>b</sup>Centro para el Desarrollo de la Nanociencia y Nanotecnología (CEDENNA) and <sup>c</sup>Departamento de Física, Universidad de Santiago de Chile, 725475 Santiago, Chile

<sup>d</sup>Departamento de Química - ICEX, Universidade Federal de Minas Gerais (UFMG),  
Campus Pampulha, 31270-901 Belo Horizonte-MG, Brazil

<sup>e</sup>Universidade Federal dos Vales do Jequitinhonha e Mucuri (UFVJM), Campus JK,  
39100-000 Diamantina-MG, Brazil

Composites based on nanosized particles of magnetite and natural micro-sized zeolite were prepared and their efficiency to adsorb arsenate from aqueous systems was evaluated through kinetic data and adsorption isotherms, considering the proportion of magnetic iron oxide, composite:solution ratio and zeolite particle size. A well-crystallized nanomagnetite with an averaged particle size of 50 nm when supported on zeolite was obtained; the nanomagnetite enhances the arsenate adsorption of zeolite. The composite prepared with a nanomagnetite:zeolite mass ratio of 0.43:1 and 0.30:1 presented on zeolite milled 20 and 120 min, respectively, showed a similar adsorption capacity as that observed for pure magnetite. Supported nanomagnetite prevents risks of the nanoparticles contamination. The smaller the mean particle size of zeolite the lower the mass proportion of nanomagnetite in the composite required to reach the maximum adsorptive efficiency. Acidic conditions improve arsenate removal, in agreement with the development of positive surface charge in the composite.

**Keywords:** composites, magnetic materials, nanostructures, Mössbauer spectroscopy, surface properties

### Introduction

The geological characteristics and mining activities may often impart critical natural and anthropogenic contamination of ground and underground waters. The increasing level of arsenic on the Earth surface has been leading not only to serious environmental problems, but these are also the cause of great concerns about their direct effects on individuals, either those living in remote small communities or in densely populated urban areas of big cities.<sup>1,2</sup> In northern Chile, especially in the Antofagasta region (located approximately from 21°28' to 25°40' S), the occurrence of arsenic in ground and underground fresh waters is steadily increasing, as a consequence of the intensive mining activities. Arsenic contents in water of that region are commonly two to four times higher<sup>3,4</sup> than that upper limit (0.01 mg L<sup>-1</sup>) established

by the Chilean standard for drinking water<sup>5</sup> and several times higher<sup>6,7</sup> than that recommended (0.1 mg L<sup>-1</sup>) for agriculture irrigation.<sup>8</sup> In recent years, some studies have been reported accounting for the effects on the health of the inhabitants of that area.<sup>9,10</sup> The most frequently-occurring chemical arsenic species in ground water (pH values varying from 6 to 8) of northern Chile are H<sub>2</sub>AsO<sub>3</sub><sup>-</sup>, H<sub>3</sub>AsO<sub>3</sub> for As<sup>III</sup>, and H<sub>2</sub>AsO<sub>4</sub><sup>-</sup>, HAsO<sub>3</sub><sup>2-</sup>, for As<sup>V</sup>.<sup>11</sup> Different technological treatments have been used in an effort to remove or mitigate the biological action of this pollutant. Iron oxides are one of the most effective agents in the removal of arsenic.<sup>12-14</sup> Studies have indicated a high affinity of the iron oxides to absorb arsenic oxyanions,<sup>15,16</sup> mainly due to the surface properties and spatial molecular configuration of the arsenic oxyanions on adsorption sites, forming inner sphere complexes with iron oxides,<sup>17,18</sup> although the formation of outer-sphere complexes cannot be excluded.<sup>19</sup> However, the use of iron oxide-based materials has not always been effectively lowering

\*e-mail: carmen.pizarro@usach.cl

pollutant concentrations to levels below the upper limit concentrations officially accepted as being safe, according to recommendations by the World Health Organization.<sup>20</sup> It is then expected that increasing the surface area of the adsorbent material, which is directly contacted by the contaminant, would result in a significant increase of the remediation efficiency. This effect has been clearly reportedly observed elsewhere, in which an increase of the adsorbing arsenic capacity with decreasing magnetite particle sizes.<sup>21</sup> However, recent studies<sup>22-24</sup> have warned about the potential damage that could cause dispersing synthetic nanoparticles in the natural environment. The main purpose of this work was to propose a relatively comprehensive study regarding the synthesis of nanosized magnetite particles, to combine minor proportions of the synthetic magnetic material with a naturally-occurring aluminosilicate, taking advantage of the so-prepared composite on arsenic adsorption, thinking at preventing any more significant collateral harm to the ecosystem, on suspending the nanoparticles into water. The nanomagnetite-zeolite composites are a promising alternative to efficiently remove inorganic anions from aqueous media.

Preparing iron oxides materials to be suitably used as adsorbents in environmental remediation is a critical step to optimize cost/efficiency ratios, particularly at industrial scales.<sup>25</sup> Magnetite is widely used for many industrial and environmental applications. Even being relatively well known, its synthesis involves several specific challenges, particularly those related to control some critical properties of the final product, namely crystallinity and chemical purity, chemical stability against oxidation in air, particle sizes and morphologies distribution and magnetic structure. Small-sized magnetite tends to be readily oxidized in air and presents more crystallographic defects and lower saturation magnetization than a well crystalline bulk magnetite.

Nanomagnetite-zeolite composites were prepared and chemically characterized, in order to obtain an economically interesting, an ecological sustainable and a technologically efficient adsorbent material to remove arsenate from natural water bodies. Kinetic data, adsorption isotherm, composite content of magnetic iron oxides, composite:solution ratio and particle size of the zeolite were considered to evaluate the arsenate adsorption efficiency of composites.

## Experimental

The synthesis of magnetite was initially done through the classical procedure described in Schwertmann and Cornell.<sup>26</sup> Following this procedure, about 5 g of a magnetic solid product was obtained. The procedure involves the dissolution of 20 g of  $\text{FeSO}_4$  in 150 mL of double-distilled water at 80 °C (previously degassed with

$\text{N}_2$ ). Subsequently, 60 mL of a solution containing  $\text{KNO}_3$  (27 g  $\text{L}^{-1}$ ) and  $\text{KOH}$  (190 g  $\text{L}^{-1}$ ) were added dropwise; the reaction was kept at 80 °C under stirring for 1 h, cooling overnight at room temperature. After that, the precipitate obtained was washed with double-distilled water. Different nitrogen flow rates and stirring conditions were tested, in order to obtain as much as possible well-crystallized and stoichiometric nanosized magnetite. To evaluate the effects of four synthesis conditions, involving different nitrogen flow rates and stirring, magnetite samples were prepared. The effects of these changes were monitored with  $^{57}\text{Fe}$  Mössbauer spectroscopy, scanning electron microscopy (SEM) and magnetometer measurements.

A zeolite sample was collected from a mine located in mid-southern Chile (geographical coordinates of the sampling site: 36° 16' S 71° 40' W). The coarse grinding sample was additionally milled during 20 and 120 min, using a steel ball mill. The resulting materials were then treated so that the individual particles were coated with a layer of magnetite synthesized *in situ* corresponding to magnetite:zeolite mass ratios of 0.07:1, 0.20:1, 0.30:1, 0.43:1 and 0.53:1 (the samples were accordingly labeled MtZ7, MtZ20, MtZ30, MtZ43 and MtZ53, respectively, and followed with the codes D1, D2 or D3, denoting the support preparation on milling the zeolite component to form the composite specifically at coarse or no milling (sample D1), 20 min (D2), and 120 min (D3) milling), by converting ferrous sulfate in an alkali media containing a suspension of the zeolite under  $\text{N}_2$  atmosphere, following the previously described synthesis method for magnetite, by Schwertmann and Cornell.<sup>26</sup> The samples were characterized with respect to their particle size distributions and to specific surface area (SSA), along with chemical analysis, magnetometric measurements, powder X-ray diffraction (XRD), scanning electron microscopy and 298 K Mössbauer spectroscopy.

The relative proportion of each granulometric fraction was determined by the pipette method, basing on the sedimentation times, as given by Stoke's law,<sup>27</sup> using sodium pyrophosphate as dispersant. The SSA was determined by the method proposed by Heilman *et al.*,<sup>28</sup> which is based on the formation of a monolayer of ethylene glycol monoethyl ether (EGME) on a known mass of adsorbent. Elemental contents were determined by digesting as being 0.100 g of the dry sample with HF and *aqua regia* (10:1.5) in a microwave. The resultant digestion mixture was treated with ultra pure grade boric acid (Merck), diluted to 100 mL with water, and stored in a plastic bottle at 5 °C, prior to the chemical analysis with a Perkin Elmer 2000 DV inductively coupled plasma optical emission spectrometer (ICP-OES).

The specific sample magnetization was measured with a portable soil magnetometer. The equipment allows direct

digital readings of the magnetic moment of soil samples,<sup>29</sup> expressed in  $\text{J T}^{-1}$ . From the sample mass, the specific saturation magnetization in  $\text{J T}^{-1} \text{kg}^{-1}$  is deduced. An amount of about 0.3 g of each sample was placed into a plastic container and the saturation magnetization was obtained as the averaged value of about 30 readings.

Mössbauer spectra were collected at 298 K in constant acceleration transmission mode, with a ca. 30 mCi  $^{57}\text{Co}/\text{Rh}$  source. Data were stored in a 512-channel MCS memory unit, with Doppler velocities ranging between approximately  $\pm 10 \text{ mm s}^{-1}$ . The experimental data were fitted using Lorentzian functions, with least squares fitting procedure based on the NORMOSTM computer program; isomer shifts are quoted relative to  $\alpha\text{-Fe}$ .

Powder X-ray patterns of oriented samples were obtained with a Bruker 08 Advance instrument equipped with a  $\text{Cu-K}\alpha$  radiation source and a Ni filter with a pulse high analyzer system. The collected data were treated with the EVA® computer program. The diffractograms were compared with standards of the Joint Committee on Powder Diffraction Standards (JCPDS) database.<sup>30</sup>

Kinetic assays were carried out by shaking 0.4 g of each adsorbent material (zeolite, composites or magnetite) with 25 mL of  $100 \text{ mg L}^{-1}$  solution containing arsenic oxyanions at different times, ranging from 5 to 1440 min. Later, the reaction mixtures were filtered through a  $0.45 \mu\text{m}$ -pore diameter filter and then analyzed for the remaining arsenate concentration with ICP-OES.

Arsenate equilibrium isotherms were obtained by shaking 0.4 g of each adsorbent material with 25 mL of arsenate solution, at arsenate concentrations ranging from 1 to  $300 \text{ mg L}^{-1}$  As, in 50 mL centrifuge tubes, at  $\text{pH } 6.2 \pm 0.3$  and  $T = 25 \pm 0.2 \text{ }^\circ\text{C}$ . After shaking the centrifuge tubes with the suspension by 1 h (time established from previous kinetic assays), the reaction mixtures were filtered through a  $0.45 \mu\text{m}$ -pore membrane. The filtered solutions were analyzed for the remaining arsenate concentration with ICP-OES. Electron micrographs were obtained with a JEOL JSM-6400 SEM. Micrographs of the films were obtained with acceleration voltages of 10 and 15 kV and a magnification range of 3000 to 5400 $\times$ .

## Results and Discussion

### Magnetite, zeolite and composites preparation and characterization

#### Magnetite

The shaking conditions and  $\text{N}_2$  flow rates determined the characteristics of the final magnetite. Mechanical shaking produces a magnetite with smaller sizes than

that obtained by manual agitation. A flow of  $\text{N}_2$  at  $0.8 \pm 0.1 \text{ L min}^{-1}$  was found to be sufficient to obtain a well-crystallized magnetite. However,  $3.5 \pm 0.2 \text{ L min}^{-1}$  of  $\text{N}_2$  flow rendered a slight increase of the magnetization of the final product. From its side, the nitrogen injection system was critical to prevent the oxidation of magnetite by the atmospheric oxygen. Under optimal synthesis conditions, magnetite presented specific saturation magnetization values  $\sigma \geq 80 \text{ J T}^{-1} \text{kg}^{-1}$ , which is not far below  $\sigma$  ca.  $100 \text{ J T}^{-1} \text{kg}^{-1}$  (reference value for a pure, stoichiometric and well crystallized magnetite).<sup>31</sup> The mechanical stirring was found to be more appropriate than manual stirring for better controlling the mean diameter of magnetite nanoparticles  $\leq 80 \text{ nm}$ .

Powder X-ray diffractometry analysis (Figure 1a) indicates that the synthesized iron oxide indeed corresponds to crystallographic cubic structure (according to card No. 01-089-0691 of the JCPDS PDF-2 database) of magnetite.

The room temperature Mössbauer spectrum (Figure 1b) also revealed the characteristic pattern of a pure magnetite. Fitting parameters for the mixed valence  $\text{Fe}^{3+/2+}$  in octahedral sites: isomer shift relative to  $\alpha\text{Fe}$ ,  $0.67 \text{ mm s}^{-1}$ , and magnetic field,  $\text{Bhf} = 45.8 \text{ T}$ ; for  $\text{Fe}^{3+}$  in tetrahedral sites,  $0.28 \text{ mm s}^{-1}$  and  $\text{Bhf} = 48.9 \text{ T}$ . The relative areas (RA) ratio of the two profiles was  $\text{RAFe}_{(\text{oct})}/\text{RAFe}_{(\text{tet})} = 1.86$ , which is nearly the expected value (1.88), by assuming that the f-factor for octahedral  $^{57}\text{Fe}$  is 6% lower than in tetrahedral sites.<sup>32</sup>

SEM analysis (Figure 1c) shows crystals with the typical octahedral habit of magnetite; the distribution of particle sizes profile is centered at a mean diameter  $\phi = 77 \text{ nm}$ . From these synthesis conditions it was possible to obtain a nanosized magnetite highly magnetic and chemically stable.

#### Zeolite

Results from chemical analysis indicate that zeolite contains silicon and aluminum at a Si:Al ratio of 5:1 and 2.0 mass% iron. The XRD patterns (Figure 2a) indicate that the zeolite corresponds to rehydrated mordenite with calcium cations, with the chemical formula  $\text{Ca}_{3.4}\text{Al}_{7.4}\text{Si}_{40.6}\text{O}_{96}(\text{H}_2\text{O})_{31}$ . The Mössbauer spectrum shows that all iron detected in chemical analyses is likely paramagnetic  $\text{Fe}^{3+}$  (Figure 2b). SEM-energy dispersive X-ray spectroscopy (EDX) analyses were also taken for the zeolite sample, a typical image (Figure 2c) shows the zeolite to be non-aggregated; from the granulometric analysis, the particle size distribution corresponds to about 60 mass% of the sample with a diameter  $\phi < 20 \mu\text{m}$ . Moreover, EDX analysis indicated a Si:Al ratio similar to that obtained by chemical analysis.

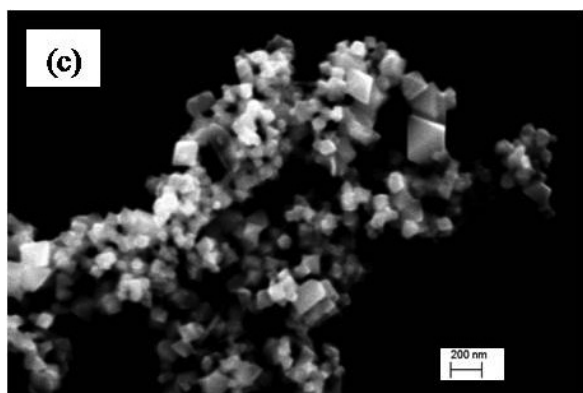
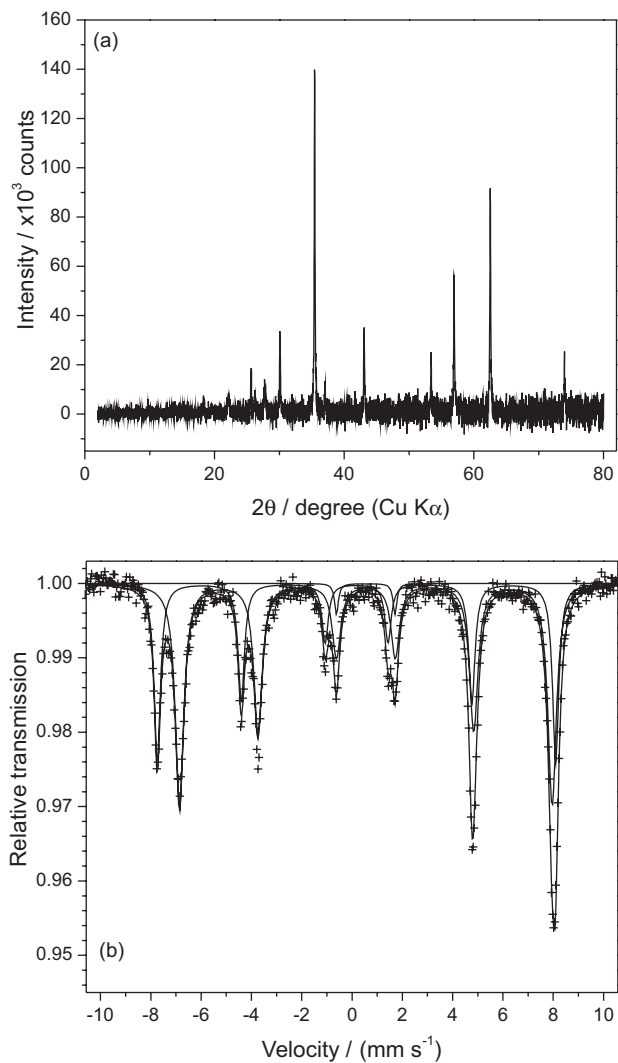


**Figure 1.** Powder X-ray pattern (a); 298 K Mössbauer spectrum (b) and SEM image (c) for synthetic magnetite.

#### Composites

The specific saturation magnetization ( $\sigma$ ) values for these magnetite-zeolite composites indicate that the magnetization increases, as expected, with the content of magnetite in the composite in a linear relationship ( $r = 0.99$ , for  $p < 0.0001$ ). In order to evaluate the purity and stoichiometry of magnetite

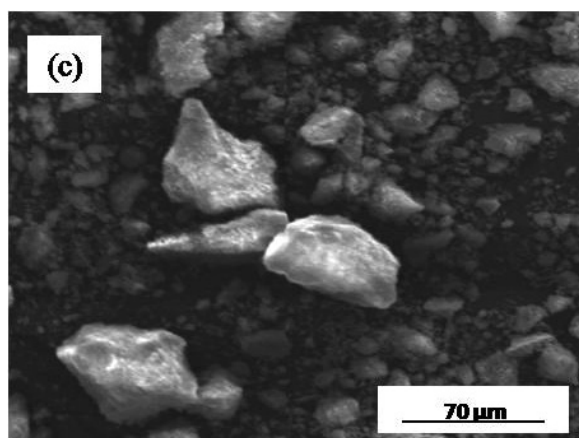
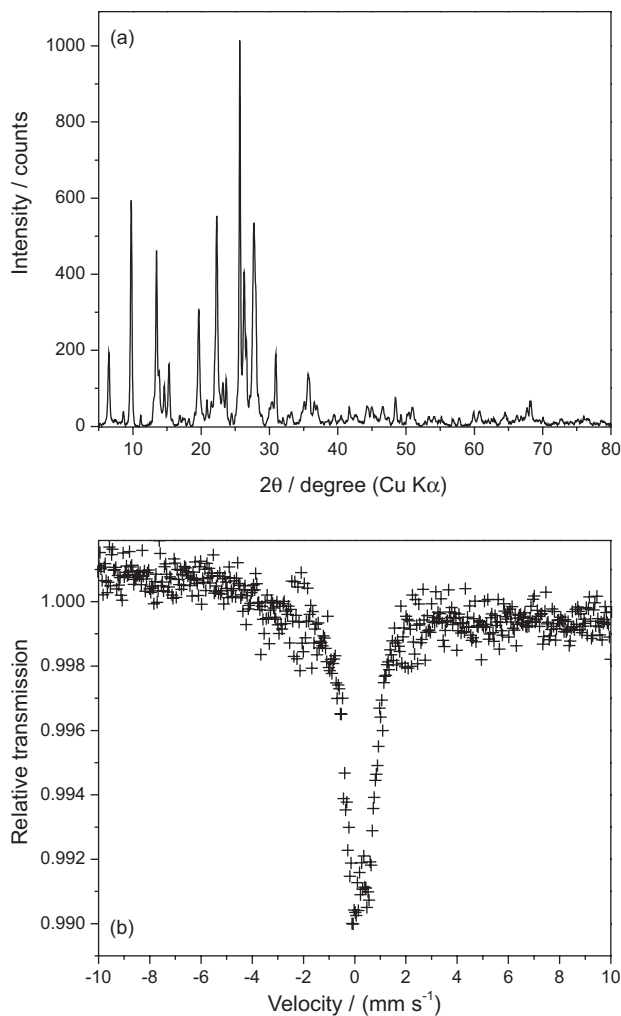


**Figure 2.** Powder X-ray pattern (a); 298 K Mössbauer spectrum (b) and SEM image (c) for zeolite sample (Z-D2).

in these composites,  $\sigma$  was recalculated considering only the synthetic iron oxide mass. From this analysis, it was observed that independently of the content of coating iron material on the zeolite, the averaged  $\sigma = 63 \pm 2 \text{ J T}^{-1} \text{ kg}^{-1}$  for the iron oxides, which correspond to a value not far below that of relatively pure and stoichiometric magnetite.

Powder X-ray patterns and Mössbauer spectra for the composites MtZ7-D2 and MtZ43-D2 are shown in Figures 3a and 3b, respectively. As a general analysis, X-ray diffractograms and Mössbauer spectra show spectral features of a stoichiometric and well-crystallized magnetite, with a particle distribution around a mean size of 50 nm (Figure 3c). Magnetite coating particles preserve the individual stoichiometric characteristics and structural properties of both zeolite and magnetite, as it can be inferred from hyperfine structures of corresponding Mössbauer spectrum (Table 1), when compared with those for the pure components (Figures 1b and 2b). No significant oxidation of Fe<sup>2+</sup> in the structure of the magnetite was observed. The Mössbauer spectrum for each of the two composites may be simply interpreted as the independent contribution of patterns due to paramagnetic Fe<sup>3+</sup> of the natural zeolite (Figure 2b) and to magnetite. From SEM-EDX analysis for composite (Figure 3c) the cubic crystallographic structure of magnetite is observed. The use of zeolite as support during the magnetite synthesis results in smaller particle sizes of magnetite than that obtained when zeolite is not present (Figures 1c and 3c).

#### Effect of magnetite:zeolite ratio

The magnetite:zeolite ratio effect was studied considering the coarse mill-grinding the zeolite during 20 min (sample Z-D2). Increasing the iron oxide content leads to an increase of the coated zeolite surface, at least up to 30 mass% of iron oxide (which corresponds to the composite MtZ30-D2); at higher iron contents clusters are formed on the surface of the particles.

Figure 4 shows the adsorption kinetics and isotherm curves for zeolite, and from 7 to 43 mass% of magnetite composites (samples MtZ7-D2 to MtZ43-D2), and for the sole magnetite. Adsorption kinetics curves show that arsenate was adsorbed before the first hour of equilibrium. Important differences in adsorption of arsenate were observed with magnetite content in the composites, particularly when iron oxide content is higher than 20 mass% (Figure 4).

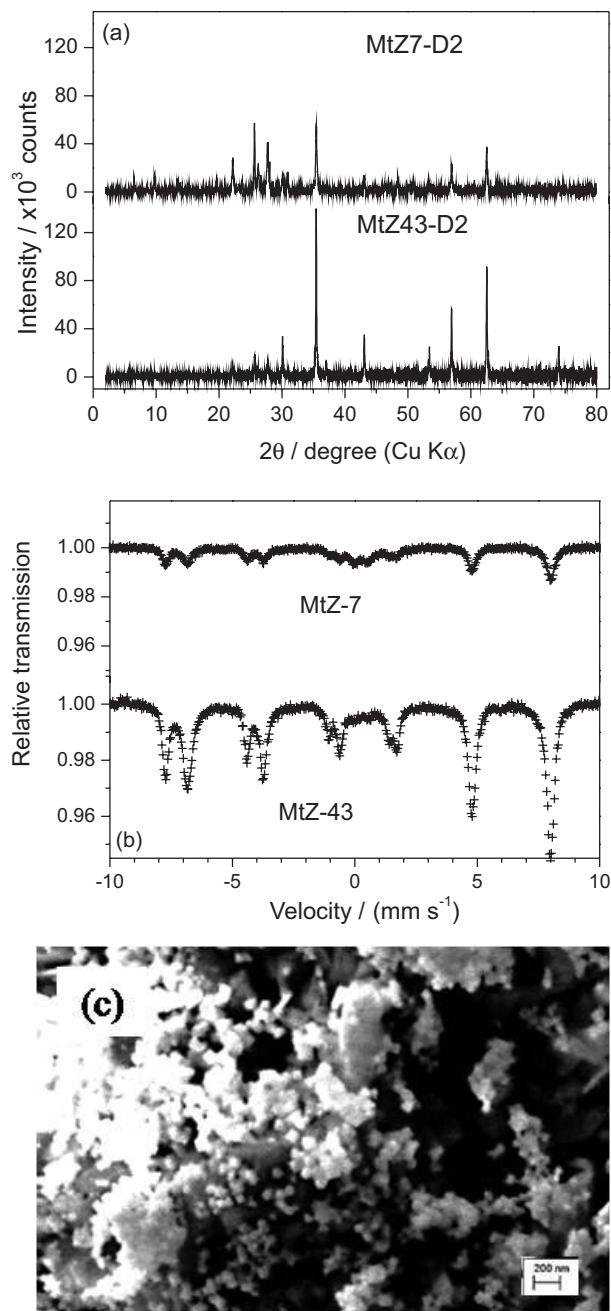


**Figure 3.** Powder X-ray patterns (a); 298 K Mössbauer spectra (b) for MtZ7-D2 and MtZ-43 composites and SEM image (c) for MtZ43-D2 composite.

**Table 1.** 298 K Mössbauer parameters for composites (MtZ7-D2 and MtZ43-D2) and synthetic nanomagnetite (Mt) samples

Sample	$\delta_{\alpha\text{Fe}}$ / (mm s <sup>-1</sup> )	$\epsilon$ / (mm s <sup>-1</sup> )	$B_{\text{hf}}$ / T	$\text{RAFe}_{(\text{oct})}/\text{RAFe}_{(\text{tet})}$
MtZ7-D2	$0.27 \pm 0.01$	$-0.02 \pm 0.01$	$48.8 \pm 0.2$	1.46
	$0.67 \pm 0.01$	$0.01 \pm 0.01$	$45.8 \pm 0.2$	–
MtZ43-D2	$0.27 \pm 0.01$	$-0.01 \pm 0.01$	$48.8 \pm 0.2$	1.82
	$0.67 \pm 0.01$	$0.02 \pm 0.01$	$45.8 \pm 0.2$	–
Mt	$0.28 \pm 0.01$	$0.00 \pm 0.01$	$48.9 \pm 0.2$	–
	$0.67 \pm 0.01$	$0.00 \pm 0.01$	$45.8 \pm 0.2$	1.86

$\delta_{\alpha\text{Fe}}$ : Isomer shift relative to  $\alpha\text{Fe}$ ;  $\epsilon$ : splitting quadrupole;  $B_{\text{hf}}$ : magnetic field;  $\text{RAFe}_{(\text{oct})}/\text{RAFe}_{(\text{tet})}$ : ratio between relative area of Fe octahedral sites ( $\text{RAFe}_{(\text{oct})}$ ) and relative area of Fe tetrahedral site ( $\text{RAFe}_{(\text{tet})}$ ).

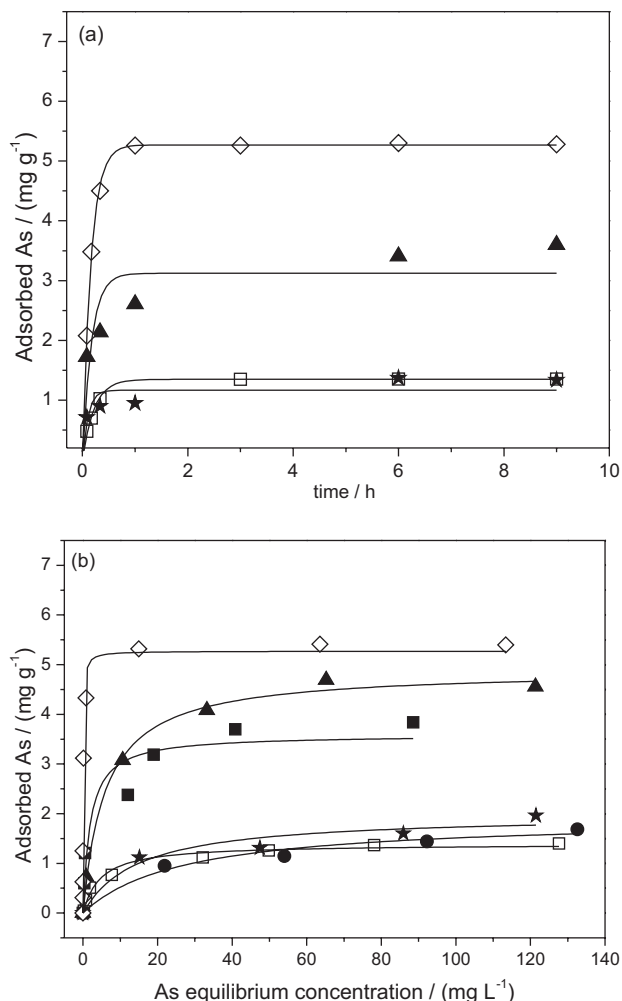


**Figure 4.** Arsenate adsorption kinetics (a) and isotherm (b) curves for natural zeolite (Z-D2 = □), composites with magnetite:zeolite mass ratios of 0.07:1, 0.20:1, 0.30:1 and 0.43:1 (MtZ7-D2 = ★, MtZ20-D2 = ●, MtZ30-D2 = ■ and MtZ43-D2 = ▲, respectively), and magnetite (Mt = ◇).

The natural zeolite has an adsorption kinetic curve similar to composites in terms of time to the equilibrium (Figure 4a), but with a comparatively low amount of adsorbed arsenate, only similar to MtZ7-D2 composite (Figure 4b); contrarily, MtZ43-D2 had a similar adsorption capacity to that observed for pure magnetite. The adsorption isotherm was well described by the Langmuir model; the maximum adsorption value for the MtZ43-D2 composite was found to be  $4.6 \text{ mg g}^{-1}$ . No arsenate desorption from composites was observed (desorption isotherm carried out on MtZ43-D2 samples, previously treated with arsenate solutions ranging from 0 to  $300 \text{ mg L}^{-1}$  of arsenate; details in Experimental). The presence of magnetite significantly increased the ability of zeolite to remove arsenic from water, the high interaction of magnetite active sites for arsenate generates the formation of mono and/or bi-dentate Fe-As complexes through a ligand exchange reaction (and,

in a lesser extent, the formation of outer sphere complexes), which results in very stable complexes.<sup>33,34</sup>

From an electrostatic point of view, iron content increases the positive surface charge of zeolite, enhancing the composites adsorption of anions. However, over 43 mass% of iron oxide, the arsenate adsorption on the surface of the composite particles does not increase significantly, presenting a maximum adsorption capacity similar to pure magnetite.

#### Effect of particle size distribution

In this study, three different particle size distributions for the zeolite were considered: (i) coarse ground material (labeled Z-D1, corresponding to the zeolite with only a gentle grinding, after it was collected from the mine); (ii) zeolite ground during 20 min (Z-D2); and (iii) zeolite ground during 120 min (Z-D3).

Samples Z-D1, Z-D2 and Z-D3 were used to prepare the 30 mass% iron oxide composites (MtZ30-D1, MtZ30-D2 and MtZ30-D3). Specific surface area (SSA, attributed to total surface involving internal + external surface), and particle size distribution for the zeolite samples (D1-D3) and MtZ30 (D1-D3) composites are shown in Table 2.

**Table 2.** Specific surface area and granulometric breakdown for zeolite and MtZ30 composite samples

	Zeolite		
	Z-D1	Z-D2	Z-D3
SSA / ( $\text{m}^2 \text{g}^{-1}$ )	$60 \pm 1$	$108 \pm 1$	$121 \pm 1$
Particle size ( $\phi$ ) / $\mu\text{m}$	Mass / %		
> 53	$91.8 \pm 0.1$	$29.5 \pm 0.1$	$18.1 \pm 0.1$
53-20	$0.2 \pm 0.1$	$9.0 \pm 0.3$	$5.4 \pm 0.1$
20-2	$7.2 \pm 0.1$	$37.7 \pm 0.2$	$44.3 \pm 0.2$
< 2	$0.8 \pm 0.1$	$23.8 \pm 0.1$	$32.2 \pm 0.1$
	Composite		
	MtZ30-D1	MtZ30-D2	MtZ30-D3
SSA / ( $\text{m}^2 \text{g}^{-1}$ )	$33 \pm 1$	$39 \pm 1$	$47 \pm 1$
Particle size ( $\phi$ ) / $\mu\text{m}$	Mass / %		
> 53	$93.6 \pm 0.1$	$34.2 \pm 0.1$	$32.1 \pm 0.1$
53-20	$2.3 \pm 0.1$	$20.9 \pm 0.1$	$13.1 \pm 0.2$
20-2	$2.6 \pm 0.1$	$42.7 \pm 0.1$	$47.8 \pm 0.1$
< 2	$1.5 \pm 0.1$	$2.2 \pm 0.1$	$7.1 \pm 0.1$

SSA: Specific surface area.

Sample Z-D1 is a coarse material with about 90% of its particles sizing over  $53 \mu\text{m}$ ; the Z-D2 and Z-D3 samples have particle sizes ranging from 2 to  $20 \mu\text{m}$  (Table 2). As result of the preparation procedures, samples of the

composites MtZ30-D2 and MtZ30-D3 increased about 13 and 8% the 2-20  $\mu\text{m}$  particle size range and decreased the finest fraction ( $< 2 \mu\text{m}$ ). As result of the increasing zeolite milling time the composite prepared from Z-D3 increases about 20% the  $< 20 \mu\text{m}$  particles content with respect to that prepared with Z-D2. Consequently, there is an important increase in SSA from Z-D1 to Z-D3 (Table 2), but the SSA of zeolite-nanomagnetite decreased, as result of the iron oxides coating during preparation of composites.

While the SSA of zeolite increased about 12%, following the increasing grinding time (Z-D1 vs. Z-D2), the SSA decreased by more than 35% for the corresponding composites, showing a reduction of the inner surface compared to zeolite, as result of the iron oxide coating. However, if composites are compared, the SSA of MtZ30-D3 is about 20% higher than that for MtZ30-D2 (Table 2), which agrees with the analysis of the particle size distribution.

#### Kinetic curves and adsorption isotherms

From Figure 5, a rapid increase of the adsorption capacity in all samples is observed in the first 30 min, reaching the maximum adsorption at 1 h, independently of the amount and type of adsorbent used. The same behavior has been observed for arsenic adsorption on other iron materials surfaces.<sup>35</sup> Independently of solid:solution ratio, the arsenate adsorption efficiency follows the sequence Z-D1  $<$  MtZ30-D1  $\leq$  Z-D2  $<$  Z-D3  $<$  MtZ30-D2  $<$  MtZ30-D3  $\leq$  Mt.

The arsenic adsorptions kinetics (Figure 5, Table 3) was well described by the pseudo-first order model.<sup>36,37</sup> This model relates the adsorbed concentration as a function of time (equation 1).

$$\log(q_e - q_t) = \log(q_e) - \frac{k_1}{2.303} t \quad (1)$$

where  $q_t$  is the adsorbed arsenate at time ( $t$ ) and  $q_e$  is the amount adsorbed at equilibrium;  $k_1$  is the first order kinetics constant which can be estimated from a plot of  $\log(q_e - q_t)$  vs.  $t$ .

Figure 6 shows the arsenate adsorption isotherms fitted by Langmuir approach;<sup>38</sup> resulting parameters from fitting curves for the zeolite, the composites and the magnetite samples are presented in Table 4. The Langmuir approach relates the adsorbed concentration as a function of the equilibrium concentration; the expression is given by:

$$q = \frac{1}{K_L q_m} + \frac{C}{q_m} \quad (2)$$

where  $q$  is the amount of the adsorbed arsenate ( $\text{mg g}^{-1}$ ) and  $q_m$  is the maximum adsorption capacity ( $\text{mg g}^{-1}$ ),  $K_L$  is

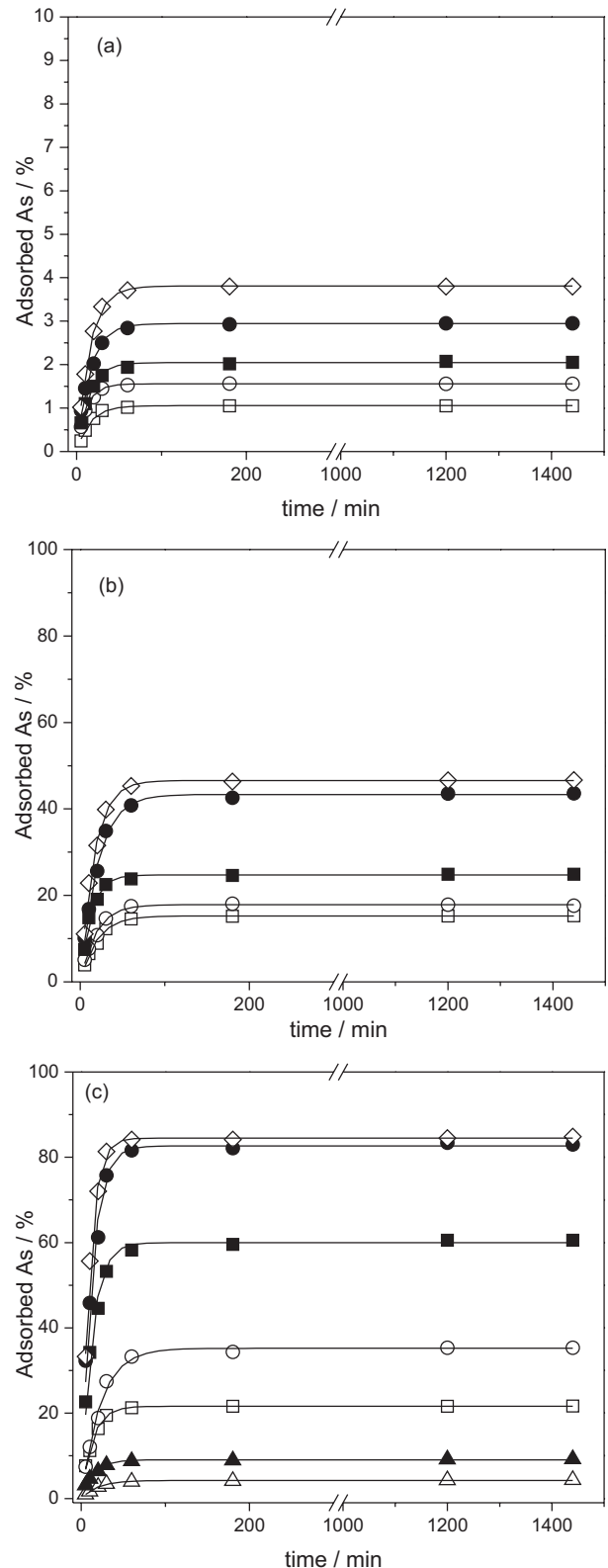


**Figure 5.** Experimental data (symbols) and fitted curves (lines) for arsenate adsorption of kinetics carried out on magnetite (Mt = ◇), natural zeolite (Z-D1 = △, Z-D2 = □, Z-D3 = ○), and composites considering particle size distribution (MtZ30-D1 = ▲, MtZ30-D2 = ■, MtZ30-D3 = ●) and adsorbent concentration:  $0.5 \text{ g L}^{-1}$  (a);  $5 \text{ g L}^{-1}$  (b) and  $16.0 \text{ g L}^{-1}$  (c). A different scale was considered for ordinate axis in graph (a) with respect to graphs (b) and (c).

**Table 3.** Parameters for the pseudo first order model for arsenate adsorption on zeolite, MtZ30 composite (with different particle size distribution), and magnetite (Mt)

Parameter	Zeolite			
	Z-D1	Z-D2	Z-D3	
$k_1 / \text{min}^{-1}$	$0.05 \pm 0.01$	$0.07 \pm 0.00$	$0.04 \pm 0.00$	
$r^2$	0.99	0.99	0.99	
Parameter	Composite			Mt
	MtZ30-D1	MtZ30-D2	MtZ30-D3	
$k_1 / \text{min}^{-1}$	$0.07 \pm 0.00$	$0.08 \pm 0.00$	$0.08 \pm 0.00$	$0.09 \pm 0.00$
$r^2$	0.99	0.98	0.98	0.99

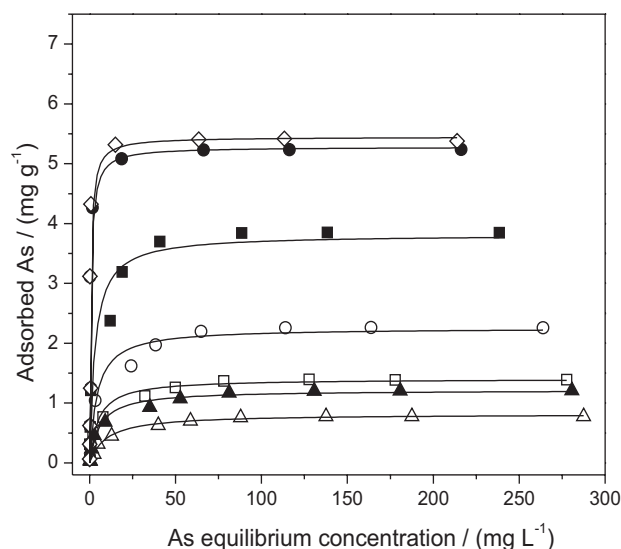
$k_1$ : First order kinetics constant;  $r^2$ : coefficient of determination.

the Langmuir constant and  $C$  the concentration ( $\text{mg L}^{-1}$ ) of arsenate. From a plot of  $q$  vs.  $C$  it is possible to determine  $K_L$  and  $q_m$ .

The arsenate adsorption is described by an L-type curve, which is characteristic of a high adsorption affinity system,<sup>39</sup> associated with a chemisorption process ( $> 20 \text{ kcal mol}^{-1}$ ). The MtZ30-D3 composite presents a similar adsorption maximum but a lower affinity than that observed for the sole magnetite, which presents the highest affinity for arsenate (Table 4).

The arsenate adsorption by magnetite presents an H-type curve, which is an extreme case of L-type adsorption curve.<sup>39</sup> For zeolite, the maximum of arsenate adsorption,  $q_m$ , increases about 61% for the grinding time increasing from 20 to 120 min.

Coating with iron oxide significantly improves the arsenate adsorption capacity; thus, for MtZ30 composites  $q_m$  increases 272 and 225% for D2 and D3 zeolite, respectively, if compared with the sole zeolite in the same grinding time conditions, and even more significantly (623%), if compared with the coarse zeolite (Table 4). Thus, the arsenic adsorption capacity increases with the iron oxide content of composites, but also with grinding

**Figure 6.** Experimental data (symbols) and Langmuir fitted curves (lines) for arsenate adsorption isotherms carried out on magnetite (Mt =  $\diamond$ ), natural zeolite (Z-D1 =  $\triangle$ , Z-D2 =  $\square$ , Z-D3 =  $\circ$ ), and composites with magnetite:zeolite mass ratios 0.30:1 prepared with zeolite milled at D1, D2 and D3 conditions (MtZ30-D1 =  $\blacktriangle$ , MtZ30-D2 =  $\blacksquare$ , MtZ30-D3 =  $\bullet$ ).

time, related to an increase of SSA of samples as result of a reduction of particle size (Table 2).

**Table 4.** Langmuir parameters for arsenate adsorption isotherms carried out on magnetite (Mt), zeolite (Z-D1, Z-D2 and Z-D3) and MtZ30 composite samples with different particle size distribution (MtZ30-D1, MtZ30-D2 and MtZ30-D3)

Parameter	Zeolite			
	Z-D1	Z-D2	Z-D3	
$q_m / (\text{mg g}^{-1})$	$0.8 \pm 0.0$	$1.4 \pm 0.0$	$2.3 \pm 0.1$	
$K_L / (\text{L mg}^{-1})$	$0.1 \pm 0.0$	$0.2 \pm 0.0$	$0.2 \pm 0.1$	
$r^2$	0.99	0.98	0.94	
Parameter	Composite			Mt
	MtZ30-D1	MtZ30-D2	MtZ30-D3	
$q_m / (\text{mg g}^{-1})$	$1.2 \pm 0.0$	$3.8 \pm 0.2$	$5.1 \pm 0.3$	$5.2 \pm 0.2$
$K_L / (\text{L mg}^{-1})$	$0.2 \pm 0.0$	$0.3 \pm 0.1$	$8.0 \pm 0.9$	$11.6 \pm 0.9$
$r^2$	0.98	0.95	0.96	0.95

$q_m$ : Maximum of arsenate adsorption;  $K_L$ : Langmuir constant;  $r^2$ : coefficient of determination.

The maximum arsenate adsorption for composites MtZ30-D2, MtZ43-D2 and D3-MtZ30 (3.81, 4.6 and 5.1 mg g<sup>-1</sup>, respectively) is comparable to those previously reported for nanomagnetite (3.7 mg g<sup>-1</sup>, with a particle size of 20 nm)<sup>40</sup> and for a nanomagnetite-nanomagnetite mixture (5.9 mg g<sup>-1</sup>, with particle size ranging from 20 to 40 nm),<sup>41</sup> but with a shorter equilibration time (one hour *vs.* three hours). In all cases, the adsorption isotherms can be fitted by the Langmuir model. The MtZ30-D3 composite presents a similar maximum adsorption of arsenate to that observed for synthetic nanomagnetite (5.1 *vs.* 5.2 mg g<sup>-1</sup>, Table 4).

#### Effect of the composite:solution ratio on arsenate adsorption

The importance of composite:solution ratio on arsenate kinetic and adsorption efficiency was evaluated for MtZ30-D2 composite, considering ratios of 0.5, 5.0 and 16.0 g of composite suspended in 1 L of aqueous solution containing 100 mg L<sup>-1</sup> of arsenate (Figure 5). The kinetics rate is not affected by the composite:solution ratio, from 98 to 100% of the composites maximum theoretical adsorption sites were occupied (3.81 mg g<sup>-1</sup>, after Langmuir model parameter  $q_m$ , Table 4), making it easy to estimate the amount of composite required to remove arsenate. In terms of efficiency, acidic conditions improve arsenate adsorption, in agreement with the generation of positive surface charge on the -Fe-OH active surface sites of composite, characterized by pH dependent surface charge.

Summarizing, nitrogen flow control is essential to prevent excessive Fe<sup>2+</sup> oxidation during the synthesis of magnetite. Under optimal conditions, synthetic magnetite presents magnetic saturation values  $\sigma \geq 80 \text{ J T}^{-1} \text{ kg}^{-1}$ . The mechanical stirring is more efficient than the manual stirring, allowing the synthesis of magnetite nanoparticles of  $\leq 80 \text{ nm}$  of mean diameter size. A stoichiometric and well-crystallized magnetite in the composite samples was obtained, with a particle size distribution smaller than pure magnetite, centered to a mean particle size of 50 nm.

Nanomagnetite coating significantly increases the arsenate adsorption capacity of zeolite, due to the high Fe-As affinity. The iron oxide in composites increases the availability of positive charges on the surface of particles favoring, from an electrostatic point of view, the interaction of arsenate with surface active sites.

The grinding procedure tends to increase the SSA of zeolite. Despite of reduction of SSA after iron oxide coating, the adsorption of arsenate is significantly increased with coating. The composite prepared with zeolite milled for 20 min and magnetite:zeolite mass ratio of 0.43:1 (ZMt43-D2) and the composite with mass ratio of 0.30:1, with the zeolite milled for 120 min (ZMt30-D3), present a

similar arsenate adsorption capacity as pure nanomagnetite, but it prevents the transport of potentially dangerous nanoparticles into the water and soil environment. The lower the particle size of the zeolite the higher the arsenate adsorption capacity of composites.

## Conclusions

This comprehensive study was devoted to optimize the laboratory preparation of nanomagnetite-zeolite composites, in an attempt to use these adsorbing magnetic materials to remove arsenate from water. Supporting nanomagnetite particles on the natural zeolite has economical, technological and environmental advantages. The starting materials, the synthetic magnetite and the natural silicate (zeolite) are relatively affordable, making the composite attractive to be used in industrial scale. From the technological point of view, the use of composites formed with the magnetic iron oxide allows the adsorbent to be magnetically removed from the water medium. Environmentally, the proposed adsorbing magnetic system represents a prospective procedure to clean larger natural bodies of water being affected with chemical contamination, particularly arsenic anions.

From a kinetic point of view, a rapid increase of the arsenate adsorption capacity in all composite is observed in the first 30 min with respect to zeolite, reaching the maximum of adsorption about 1 h. The arsenate adsorption on Fe-OH active surface sites is characteristic of a high adsorption affinity system associated with a chemisorption process. The MtZ40-D2 and MtZ30-D3 composites present a similar adsorption maximum but a lower affinity than that observed for the nanomagnetite, which presents the highest affinity for arsenate. Thus, the arsenate adsorption capacity increases with the iron oxide content of composites, but also with grinding time, related to an increase of SSA of samples as result of a reduction in particle size.

Regarding its adsorbing efficiency, only 30 to 40% of supported magnetite is needed to get the same specific response as found for pure nanomagnetite, additionally, the use of micrometric composite prevents eventual contamination of natural systems with nanoparticles as would be with pure nanomagnetites. It must be emphasized that the reduction of any harmful effect to the environment must be a critical criterion to choose a remediation system to clean contaminated water with arsenic anions.

## Acknowledgements

Work financially supported by DICYT-USACH 021242PA, CEDENNA FB-0807 (Chile), CNPq

(Brazil; grants No. 302479/2010-4 and PROSUL No. 490096/2010-7) and FAPEMIG (Brazil; including No. PPM 00419-10). CAPES (Brazil) grants the PVNS professorship to J. D. F. at UFVJM.

## References

- Palacios, J.; Nwokocha, C. R.; Cifuentes, F.; *World J. Pharmacol.* **2014**, *3*, 18.
- Zheng, L.; Kuo, Ch.; Fadrowski, J.; Agnew, J.; Weaver, V. M.; Navas-Acien, A.; *Curr. Environ. Health Rep.* **2014**, *1*, 192.
- Cifuentes, F.; Bravo, J.; Norambuena, M.; Stegen, S.; Ayavire, A.; Palacios, J.; *Int. J. Toxicol.* **2009**, *28*, 534.
- Palacios, J.; Roman, D.; Cifuentes, F.; *Biol. Trace Elem. Res.* **2012**, *148*, 224.
- <http://www.bvsde.paho.org/bvsacg/e/cd-cagua/ref/text/42.pdf> accessed in June 2015.
- Leybourne, M. I.; Cameron, E. M.; *Chem. Geol.* **2008**, *247*, 208.
- Romero, L.; Alonso, H.; Campano, P.; Fanfani, L.; Cidu, R.; Dadea, C.; Keegan, T.; Thornton, I.; Farago, M.; *Appl. Geochem.* **2003**, *18*, 1399.
- [http://ciperchile.cl/pdfs/11-2013/norovirus/NCh1333-1978\\_Mod-1987.pdf](http://ciperchile.cl/pdfs/11-2013/norovirus/NCh1333-1978_Mod-1987.pdf) accessed in June 2015.
- Román, D. A.; Pizarro, I.; Rivera, L.; Cámara, C.; Palacios, M. A.; Gómez, M. M.; Solar, C.; *Hum. Exp. Toxicol.* **2010**, *30*, 1150.
- Román, D. A.; Pizarro, I.; Rivera, L.; Torres, C.; Ávila, J.; Cortés, P.; Gill, M.; *BMC Res. Notes.* **2012**, *5*, 207.
- Ravenscroft, P.; Brammer, H.; Richards, K.; *Arsenic Pollution: A Global Synthesis*, 1<sup>st</sup> ed.; John Wiley & Sons: West Sussex, 2009.
- [http://water.epa.gov/drink/info/arsenic/upload/2005\\_11\\_10\\_arsenic\\_treatments\\_and\\_costs.pdf](http://water.epa.gov/drink/info/arsenic/upload/2005_11_10_arsenic_treatments_and_costs.pdf) accessed in June 2015.
- Jeon, C. S.; Baek, K.; Oh, Y. K.; Lee, S. D.; *J. Hazard. Mater.* **2009**, *16*, 804.
- Mohana, D.; Pittman Jr., C. U.; *J. Hazard. Mater.* **2007**, *142*, 1.
- Hartley, W.; Edwards, R.; Lepp, N. W.; *Environ. Pollut.* **2004**, *131*, 495.
- Kim, E. J.; Yoo, J. C.; Baek, K.; *Environ. Pollut.* **2014**, *186*, 29.
- Farrell, J.; Chaudhary, B. K.; *Environ. Sci. Technol.*, **2013**, *47*, 8342.
- Zuo, J. C.; Tong, S. R.; Yu, X. L.; Wu, L. Y.; Cao, C. Y.; *J. Hazard. Mater.* **2012**, *235-236*, 336.
- Catalano, J. G.; Park, C.; Fenter, P.; Zhang, Z.; *Geochim. Cosmochim. Acta* **2008**, *72*, 1986.
- [http://whqlibdoc.who.int/ehc/WHO\\_EHC\\_224.pdf](http://whqlibdoc.who.int/ehc/WHO_EHC_224.pdf) accessed in June 2015.
- Yean, S.; Cong, L.; *J. Mater. Res.* **2005**, *20*, 3255.
- Auffan, M.; Rose, J.; Bottero, J.; Lowry, G. V.; Jolivet, J. P.; Wiesner, M. R.; *Nat. Nanotechnol.* **2009**, *4*, 634.
- Kumar, A.; Pandey, A. K.; Singh, S.; Shanker, R.; Dhawan, A.; *Free Radical Biol. Med.* **2011**, *51*, 1872.
- Levard, C.; Hotze, E. M.; Lowry, G. V.; Brown, G. E.; *Environ. Sci. Technol.* **2012**, *46*, 6900.
- Cornell, R. M.; Schwertmann, U.; *The Iron Oxides: Structure, Properties, Reactions, Occurrences and Uses*, 2<sup>nd</sup> ed.; Wiley-VCH: New York, 2003.
- Schwertmann, U.; Cornell, R. M.; *Iron Oxides in the Laboratory: Preparation and Characterization*, 2<sup>nd</sup> ed.; Wiley-VCH: New York, 2000.
- Jackson, M. L.; *Soil Chemical Analysis*, 2<sup>nd</sup> ed.; Parallel Press, University of Wisconsin-Madison Libraries: Madison, 1985.
- Heilman, M. D.; Carter, D. L.; Gonzalez, C. L.; *Soil Sci.* **1965**, *100*, 409.
- Coey, J. M. D.; Cugat, O.; McCauley, J.; *Rev. Fis. Apl. Instrum.* **1992**, *7*, 25.
- Joint Committee on Powder Diffraction Standards (JCPDF) Powder Diffraction File (PDF); International Centre for Diffraction Data: Newton Square, 2004.
- Coey, J. M. D. In *Iron in Soils and Clay Minerals*; Stucki, J. W.; Goodmann, B. A.; Schwertmann, U., eds.; D. Reidel: Dordrecht, 1988.
- Sawatzky, G. A.; Van Der Woude, F.; Morrish, A. H.; *Phys. Rev.* **1969**, *187*, 747.
- Couture, R. M.; Rose, J.; Kumar, N.; Mitchell, K.; Wallschläger, D.; Van Cappellen, P.; *Environ. Sci. Technol.* **2013**, *47*, 5652.
- Gou, X.; Du, Y.; Chen, F.; Park, H. S.; Xie, Y.; *J. Colloid Interface Sci.* **2007**, *314*, 427.
- Kanel, S. R.; Manning, B.; Charlet, L.; Choi, H.; *Environ. Sci. Technol.* **2005**, *39*, 1291.
- Azizian, S.; *J. Colloid Interface Sci.* **2004**, *276*, 47.
- Cáceres-Jensen, L.; Rodríguez-Becerra, J.; Escudey, M.; Barrientos-Poblete, L.; Castro-Castillo, V.; Parra-Rivero, J.; Flores-Díaz, Y.; Rojas-Avilez, L.; *J. Hazard. Mater.* **2013**, *262*, 602.
- Langmuir, L.; *J. Am. Chem. Soc.* **1918**, *40*, 1361.
- Sposito, G.; *The Chemistry of Soils*, 2<sup>nd</sup> ed.; Oxford University Press: New York, 2008.
- Chowdhury, S. R.; Yanful, E. K.; *Water Environ. J.* **2011**, *25*, 437.
- Chowdhury, S. R.; Yanful, E. K.; Pratt, A. R.; *Environ. Earth Sci.* **2011**, *64*, 411.

Submitted: April 16, 2015

Published online: July 3, 2015